Biogeosciences Discuss., 10, 14685–14714, 2013
www.biogeosciences-discuss.net/10/14685/2013/
doi:10.5194/bgd-10-14685-2013

Biogeosciences Discussions
Open Access

Mechanism for initiation of the offshore phytoplankton bloom in the Taiwan Strait during winter: a physical–biological coupled modeling study

J. Wang[1], **H. Hong**[1], **Y. Jiang**[1], **and X.-H. Yan**[1,2]

[1]State Key Laboratory of Marine Environmental Science, Xiamen University, Xiamen 361005, Fujian, China
[2]College of Earth, Ocean and Environment, University of Delaware, Newark, Delaware, 19716, USA

Received: 31 July 2013 – Accepted: 20 August 2013 – Published: 5 September 2013

Correspondence to: Y. Jiang (ywjiang@xmu.edu.cn)

Published by Copernicus Publications on behalf of the European Geosciences Union.

Abstract

In situ observations showed phytoplankton blooms appear during winter in the Taiwan Strait (TWS), but the mechanism for bloom initiation was unclear. With the use of a coupled physical–biological numerical model, we find the winter bloom is triggered by the relaxation of the northeasterly monsoon. Thus, the aim of this study is to investigate the mechanism for bloom formation using the model. The model results show the weakening of the northeasterly wind generates a current that carries the fresh eutrophic Min-Zhe coastal water (MZCW) off the west coast of the TWS; then a stable stratification is formed in the upper ocean of the western strait, which significantly limits the turbulence. Via diagnostic analysis of the model output, we illustrate that the reduced turbulence allows the phytoplankton to accumulate within the upper layer of the western strait, which leads to an increase in chlorophyll. The analysis is further verified by the critical turbulence theory about the bloom. In addition to reduced turbulence, the lag between zooplankton and phytoplankton responses to the offshore extension of the MZCW is responsible for the formation of the bloom at the front. Therefore, we propose the observed offshore bloom in winter in the TWS is induced by the stable water stratification and the biological processes during the relaxation of the northeasterly wind.

1 Introduction

The Taiwan Strait (TWS) is located in the subtropics of the western Pacific. In winter, it is dominated by the northeasterly monsoon. The cold, fresh and nutrient-rich Min-Zhe coastal water (MZCW) flows into the strait along the northwest coast of the strait; in the meanwhile the south mixing water (SMW), composed of the warm, saline and oligotrophic Kuroshio branch water and high-nutrient South China Sea subsurface water, intrudes into the strait from the Penghu Channel (Fig. 1) (Wang and Chern, 1988; Jan et al., 2002; Hu et al., 2010). Two water masses meet and form a series of fronts in the

BGD
10, 14685–14714, 2013

strait (Chang et al., 2006; Li et al., 2006); the front can shift with the circulation due to monsoon variation (Wang and Chern, 1989; Zhang et al., 2005).

In the middle of the northern strait, locations of fronts and winter blooms were found in the cruise data by Zhang and Huang (2000) and Naik and Chen (2008). Both studies noted the mechanism for the winter bloom might be complicated and associated with both physical and biological processes. In terms of biological processes, suitable temperature and nutrient conditions were important for the phytoplankton growth at the front (Zhang and Huang, 2000). However, this interpretation alone is not satisfying, due to the absence of physical processes.

With respect to the physical controls on the bloom, Sverdrup (1953) proposed bloom can occur in early spring on the condition that the mixing layer becomes shallower than a critical depth, leading to excessive phytoplankton growth compared to its depletion within the mixing layer. Huisman et al. (1999) further linked the bloom with turbulence in the ocean and proposed another important mechanism for the bloom, namely, critical turbulence; that is to say the bloom can also be triggered if the turbulence is less than a critical value. Recently, Taylor and Ferrari (2011) illustrated the shutdown of turbulence convection is a new criterion for the onset of the spring bloom. Inspired by that work, we find the observed blooms appeared during the relaxation of the northeast monsoon, which reduces the turbulence input at the surface and causes the fresh MZCW flow to veer off the western shore by geostrophic adjustment (Liao et al., 2013), enhancing the coastal stratification. Hence, a new hypothesis about the mechanism is proposed that the bloom is induced by the relaxation of the northeast wind.

In order to confirm our new hypothesis, a coupled physical–biological model was built to simulate the bloom. As only limited in situ and satellite observations are available, the coupled model can contribute to a comprehensive analysis of physical and biological effects on explosion of the bloom under the relaxed wind, and provide a mechanism for the bloom initiation. Moreover, the critical turbulence theory (Taylor and Ferrari, 2011; Huisman et al., 1999) is adopted to verify the model result.

BGD
10, 14685–14714, 2013

The in situ and satellite observations are shown in Sect. 2 to illustrate the bloom. In Sect. 3, the model configuration is described. The simulated bloom and hydrodynamic responses to the wind relaxation in winter are shown in Sect. 4 in a relaxed-wind experiment. In Sect. 5, both model results and the critical turbulence theory are used to investigate the mechanism for the bloom initiation during the relaxation of wind, and the reason for why the bloom is located at the front is interpreted. Finally, the mechanism for the bloom initiation is proposed in Sect. 6.

2 In situ and satellite observations

2.1 In situ observations

Under the strong northeast monsoon in winter, the sea state in the TWS is rough and the available in situ cruise data are almost all limited to the period of wind relaxation. The two surveys reported in Zhang and Huang (2000) and Naik and Chen (2008), including their observation stations, are re-plotted in Fig. 1b.

The winter offshore bloom in the TWS was reported first by Zhang and Huang (2000), which was found in February 1998. As shown in Fig. 2, the maximal chlorophyll appeared at the surface of Station 9803 and its concentration reached 3 mg m^{-3}. It is noticeable that the location of the bloom was coincident with that of the front between the MZCW (cold, fresh and eutrophic) and the SMW (warm, hyperhaline). This front is characterized by intensified horizontal and vertical gradients of temperature and salinity. Zhang and Huang (2000) proposed the reason for the offshore maximal chlorophyll was the appropriate temperature and adequate nutrient conditions that benefited the phytoplankton growth at the front.

A similar feature (Fig. 3) was observed by Naik and Chen (2008) in December 2001. The maximal chlorophyll was located in the upper layer of the front (Station D1) between the MZCW and the SMW. The remote sensing wind data in the TWS (Fig. 4) show that the monsoon decreased during 25 to 29 November 2001 before the ob-

BGD
10, 14685–14714, 2013

servation and again during the survey time of 3 to 4 December 2001. Because the phytoplankton can double at least once per day under appropriate conditions (Miles and He, 2010), we assume the bloom is related to the short-period relaxation of the northeast wind.

2.2 Satellite observations

Although the satellite data were missing during winter due to the cloudy sky in the TWS, we try to find some evidence to demonstrate our assumption. The satellite datasets include the 4 km, daily sea surface chlorophyll from the Moderate Resolution Imaging Spectroradiometer (MODIS) (http://oceandata.sci.gsfc.nasa.gov/MODISA/) and the wind speed at 10 m above the sea surface from the NASA Quick Scatterometer (QuickSCAT) during 2002 to 2011. Fortunately, the MODIS chlorophyll evolution in February 2004 (Fig. 5b–d) offers evidence for our assumption. The wind variation in the TWS is also shown in Fig. 5.

The wind data show the wind speed was reduced to about 5 m s^{-1} during the period of 16–21 February. Before the period of wind relaxation, the chlorophyll concentrations on 13 and 15 February were relatively low off the Fujian coast. On 22 February, the day after the wind relaxed, the concentration was anomalously high off the Fujian coast and it stretched along the strait for at least 200 km. Apart from this remote sensing evidence, the assumption that the bloom was induced by the relaxed northeastern monsoon is supported and elaborated on by the modeling experiment described next.

3 Model description and experimental design

The physical model used in this study is the Regional Ocean Model System (Shchepetkin and McWilliams, 2005). The vertical mixing coefficient was calculated by the Mellor and Yamada 2.5 (MY-2.5) turbulence closure model (Mellor and Yamada, 1982; Mellor, 2001). The model domain covers the northwestern Pacific from 93.13° E to

BGD
10, 14685–14714, 2013

147.68° E and from 8.54° S to 44.9° N (Fig. 1a), with a spatial resolution that varies from 20 km at the open boundary to 1 km in the TWS. The model was driven by climatological data at the open lateral boundaries and at the surface boundaries. The initial and boundary conditions for temperature and salinity were derived from the World Ocean Atlas 2005 (WOA-2005). The surface force fields were derived from the Atlas of Surface Marine Data 1994 (da Silva et al., 1994). Freshwater inputs were specified using monthly mean runoff data for the following rivers in the model domain: the Yangtze, Minjiang, Jiulongjiang, Hanjiang, and the Pearl River, and were treated as point sources at their appropriate locations along the coastal boundary (Fig. 1).

The biological model coupled with the physical model is the modified nitrogen-based nutrient–phytoplankton–zooplankton–detritus (NPZD) model described by Fennel et al. (2006). The initial and boundary conditions for NO_3 were derived from the WOA-2005. The chlorophyll concentration was extrapolated in the vertical direction from surface values specified by the Sea-viewing Wide Field-of-view Sensor (SeaWiFS) monthly climatological data (Morel and Berthon, 1989). The NO_3 load from the rivers was considered in the model, and the concentration was set to 50 mmol m^{-3}. More details of the physical and biological model configuration and verification can be found in Liao et al. (2013), Lin et al. (2013), and Wang et al. (2013).

After the physical model had spun up for one year since climatological 1 January, the coupled physical–biological model was integrated for four additional years. After two years of the integration, the model reached a quasi-equilibrium state (Wang et al., 2013), and the results from the last year are analyzed in this study. The simulation is defined as the climatological case, and the results represent the situation forced by strong climatological northeasterly wind ($\sim 10\,m\,s^{-1}$).

In the climatological case, the spring bloom is not reproduced due to the averaged northeasterly wind as discussed in the following section. A sensitivity case with the wind reduced by 75 % ($\sim 2.5\,m\,s^{-1}$; named the relaxed-wind case) in the TWS was carried out, which reproduced the blooms reasonably well. The modified wind was limited in the TWS (Fig. 1b) with a 100 km sponge layer, where the wind is linearly interpolated

BGD
10, 14685–14714, 2013

from the reduced wind in the TWS to the outside climatological wind according to the distance, and both cases started from the same initial condition on 15 January of the climatological case during its 4th year.

4 Model results

4.1 Chlorophyll distribution

The simulated surface chlorophyll distributions in the two cases are shown in Fig. 6. In the climatological case, the model reaches a relatively stable state under the climatological northeasterly wind ($\sim 10\,m\,s^{-1}$); the chlorophyll distribution varies slightly as shown by the results on the 3rd and 6th days. The chlorophyll concentration is relatively low and decreases off the western shore of the TWS, where the maximum chlorophyll is $\sim 1\,mg\,m^{-3}$. By contrast, in the relaxed-wind case, the surface chlorophyll concentration in the western strait increases obviously after 3-day integration, and a maximal chlorophyll ($\sim 2\,mg\,m^{-3}$) zone appeared in the middle of the strait, off Pingtan Island (PTI) and near the Taiwan Bank (TWB) on the 6th day.

Section S1 is sampled across the strait in Fig. 6d, and the corresponding chlorophyll distribution along the section is shown in Fig. 7. Similar to the surface chlorophyll, the chlorophyll along the section is relatively stable in the climatological case; the concentration is higher at the western shore and has a well-mixed pattern due to the strong wind. In the relaxed-wind case, the chlorophyll gradually increases in the upper layer while it decreases in the lower layers, showing a stratified pattern with high chlorophyll extending off the western shore. The maximal chlorophyll appears at the surface in the middle strait, resembling the observed patterns in Figs. 2 and 3.

Therefore, both the remote sensing data and model results support our hypothesis that the bloom is triggered by the relaxation of the northeast monsoon in winter. The chlorophyll patterns show the model's capacity to reproduce the observed bloom. In Sect. 5, the mechanism of the relaxed-wind trigger will be elaborated on.

BGD
10, 14685–14714, 2013

4.2 Circulation adjustment to the relaxed wind

The circulations in the climatological and relaxed-wind cases are shown by the along- and cross-strait velocities in Fig. 8. Forced by the climatological northeasterly wind, the cold, fresh MZCW in the surface layer flows along the west coast from the north into the TWS (Fig. 8a), and the warm, saline SMW flows northward in the lower layer and the eastern strait, which is driven by the northward pressure gradient related to the Kushiro (Yang, 2007). This structure is the same as the generally accepted pattern described by Jan et al. (1998). Compared to the along-strait velocity, the cross-strait velocity is significantly weaker (Fig. 8c). Liao et al. (2013) mentioned the strong continuous northeasterly wind can sustain the MZCW along the western coast via the onshore Ekman transport.

In the relaxed-wind case, the southward MZCW becomes weaker while the northward SMW becomes stronger (Fig. 8b), under the reduced northeasterly wind. Meanwhile, without the constraint from the northeasterly wind, the MZCW can separate from the west coast and extend beyond the central TWS by geostrophic adjustment (Liao et al., 2013). Figure 8d shows the offshore velocity dominates the TWS with a maximum velocity of $0.3\,m\,s^{-1}$, which leads to the offshore movement of the MZCW (Fig. 9).

Although both cases are forced by idealized wind fields, the simulated circulations are coincident with the observations in Jan et al. (2002) and Lin et al. (2005) and the model results in Liao et al. (2013).

4.3 Intensified stratification

In the wind-relaxed case, the cold, fresh MZCW along the Chinese coast veers offshore, forming a stable stratification with the maximum vertical gradient at ~20 m depth (Fig. 9). The stable stratification is also seen in the observation (Figs. 2 and 3), and the distributions of temperature, salinity and NO_3 along section S1 on the 3rd day are similar to the observations. On the 6th day in the relaxed-wind case, the upper layer is well

BGD
10, 14685–14714, 2013

stratified and the maximal chlorophyll appears at the surface along the front at ~80 km between the MZCW and the SMW (Figs. 7d and 9).

5 Discussion

From the sensitivity experiment, it is found that the winter bloom can be triggered by the relaxed wind, which causes the MZCW to veer offshore, forming a stable stratification in the upper ocean. How does the relaxed wind induce the bloom, and what are the contributions of the relaxed wind and stratification? These questions are answered by the following modeling diagnostic analysis.

5.1 Diagnostic analysis of the bloom

A deep understanding of the physical and biological effects on the bloom could be achieved by a diagnostic analysis of the chlorophyll conservation in Eq. (1). The left-hand side of the equation is the net changing rate of chlorophyll. The right-hand side includes diffusion rate (including both horizontal and vertical diffusion rates, with the latter dominating) and net biological rate (including phytoplankton growth and depletion rates). The depletion contains predation by zooplankton and phytoplankton mortality.

$$\underbrace{\mathrm{dChl}\ a/\mathrm{d}t}_{\text{net rate}} = \underbrace{K_\mathrm{T}\nabla^2\mathrm{Chl}\ a}_{\text{diffusion}} + \underbrace{\mu\cdot\mathrm{Chl}\ a - (g\cdot\mathrm{Zoop} + m\cdot\mathrm{Chl}\ a)}_{\text{net biological rate}}, \quad (1)$$

where Chl *a* and Zoop are the concentrations of chlorophyll and zooplankton, respectively, K_T the diffusion coefficient, μ the growth rate of phytoplankton, g he grazing rate by zooplankton, and m the mortality rate of phytoplankton.

Figure 10a and b show the vertical section of net biological rate in Eq. (1). The zero contour represents the compensation depth where the rates of growth and depletion are balanced with each other. Above this depth the net biological rate is positive, meaning the phytoplankton growth rate is faster than that of depletion (including predation

BGD
10, 14685–14714, 2013

by zooplankton and mortality); below this depth, because of light limitation, the growth rate of phytoplankton is less than that of depletion, resulting in negative net biological rates

In addition to biological effects, the chlorophyll distribution is also controlled by the diffusion effect as shown in Fig. 10c and d. The vertical mixing coefficient is shown in Fig. 11. Under the strong northeasterly wind forcing in the climatological case, the vertical diffusion rate is negative in the upper ocean and positive in the lower layer (Fig. 10c), which means the intensified mixing (Fig. 11a) transports the increased chlorophyll in the surface layer downward. When the wind is relaxed, the vertical diffusion rate of the phytoplankton (Fig. 10d) decreases significantly, due to reduced mixing coefficient (Fig. 11b). Associated with Fig. 9, it can be found that the reduced mixing in the upper ocean is mainly due to the enhanced stratification related to the fact that the MZCW veers offshore, while the decrease of turbulence input in the surface layer related to the relaxed-wind stress is secondary. In Fig. 11b, the surface diffusion coefficient at 0–100 km decreases to 10^{-3}–10^{-2} $m^2 s^{-1}$ due to the relaxed-wind stress, while the coefficient in the stratified layer decreases significantly to 10^{-6}–10^{-5} $m^2 s^{-1}$ in the western part of section S1. Above all, the weak mixing process caused by the veering offshore of the MZCW reduces the downward transportation of phytoplankton in the relaxed-wind case.

Combining the physical and biological effects, the positive rate of net biological increase in the upper ocean is largely counteracted by the negative rate of diffusion in the climatological case (Fig. 10e): the growth of phytoplankton in the upper ocean is immediately mixed downward into the lower layers to balance the depletion, which leads to the chlorophyll being relatively stable with a low concentration in this case (Fig. 7a and b).

The balance cannot be kept in the relaxed-wind case, in which the net biological rate in the upper layer (Fig. 10b) overcomes the diffusion rate (Fig. 10d), resulting in a positive net rate (Fig. 10f) in Eq. (1). As a result, the chlorophyll increases gradually in the upper layer, especially at the front between the MZCW and the SMW, where the

BGD
10, 14685–14714, 2013

net biological rate of chlorophyll is maximal. The reason for the maximal rate appearing at the front will be explained in Sect. 5.3.

The diagnostic result of the bloom is coincident with the observation in the upper ocean by Lewis et al. (1984) and the bloom theory proposed by Huisman et al. (1999) and by Taylor and Ferrari (2011) that the weakened turbulence reduces the vertical mixing and the phytoplankton can accumulate in the upper ocean where more light is available for efficient photosynthesis.

5.2 Application of critical turbulence theory

Model sensitivity test and diagnostic analysis show the mechanism of the bloom qualitatively: the relaxed wind triggers the cold, fresh, nutrient-rich MZCW to veer off the Chinese mainland coast, forming a stable stratification and thus leading to the bloom at the front during winter. How the stratification/turbulence leads to the boom can be accessed quantitatively using the solution of critical turbulence in a two-layer model proposed by Taylor and Ferrari (2011):

$$K_{cr} = h^2 \frac{(\mu_0 - m)^2}{m}, \quad (2)$$

where K_{cr} is the critical turbulence, h the depth of the upper layer (10 m in this study), μ_0 local maximal growth rate of phytoplankton, and m the depletion rate of phytoplankton.

The theory is based on the assumption that there are enough nutrients, and the phytoplankton growth is light-limited only. According to this theory, when the vertical turbulent diffusion coefficient is less than K_{cr}, there will be a bloom. Hence, our analysis is limited in the western part of section S1 in that the nutrient concentration is ample in the MZCW. According to the depth above which the bloom occurs in Fig. 7, the vertically averaged diffusion coefficient in the top 10 m layer is plotted as the dashed line, and the calculated critical turbulence is plotted as the solid line in Fig. 12.

In the climatological case, the turbulence is larger than the critical turbulence in the western part of the section, and the biological increase rate of phytoplankton is bal-

BGD
10, 14685–14714, 2013

anced by the downward mixing rate, preventing the phytoplankton from blooming. During the relaxation of the wind, the turbulence in the upper layer is smaller than the critical turbulence; therefore the net biological rate is larger than the downward mixing rate, leading to phytoplankton accumulation in the upper layer and thus the bloom.

5.3 Effect of biological processes on the bloom at the front

The discussion above illustrates the reduced turbulence mixing triggers the chlorophyll increase in the upper layer of the western strait after the wind is relaxed. The horizontal distributions of the chlorophyll show the maximal concentration appears along the front (Figs. 6d, 7d and 9). Here, we will study the mechanism for the enhanced chlorophyll at the front.

When the MZCW veers off the mainland coast, it carries abundant nutrients toward the middle of the strait, which benefits the growth of the phytoplankton in the stratified upper layer and the development of zooplankton subsequently. The evolutions of temperature, NO_3, chlorophyll, and zooplankton can be illustrated by their surface distributions along section S1 in Fig. 13 within six model days (15 to 21 January).

At the beginning (15 January) of the simulation in the relaxed-wind case, the maximal phytoplankton and zooplankton are located in the coastal zone, which is the initialization field of this case and represents the quasi-steady-state solution of the climatological case. When the wind is relaxed, the nutrients are gradually transported off the coast (Figs. 9 and 13b); correspondingly, the maximum chlorophyll moves from the coast on 15 January to 100 km on 21 January (Fig. 13c). In addition to the advection/transport processes, the chlorophyll increases locally due to photosynthesis. Subsequently, the zooplankton growth increases following the movement of the phytoplankton (Fig. 13d). Vectors in Fig. 13 show the movement of maximal zooplankton lags that of the maximal chlorophyll, which is known as the time lag between zooplankton and phytoplankton proposed by Franks et al. (1986).

At the near-shore position (e.g., 40 km from the coast), the chlorophyll reaches its maximum at first on 16 January, followed by the zooplankton maximum on 20 January.

BGD
10, 14685–14714, 2013

The zooplankton growth increases and limits the growth of the chlorophyll there in later days. By contrast, at the offshore location (e.g., 90 km from the coast), due to the time lag between the phytoplankton growth and zooplankton growth, the low zooplankton growth can hardly limit the phytoplankton growth, and the maximal chlorophyll appears at the front where the masses meet (Fig. 13a and b). The movement of NO_3 is slower than that of chlorophyll (Fig. 13a and b), owing to the uptake of phytoplankton.

In addition, the spatial lag between chlorophyll and zooplankton can be used to interpret the maximal biological rate at the front. Equation (1) shows the phytoplankton growth and depletion rates are proportional to the concentrations of phytoplankton and zooplankton, respectively. Figure 14 shows the patterns of phytoplankton growth and depletion rates are coincident with those of chlorophyll and zooplankton in Fig. 13, respectively. Therefore, the maximal net biological rate is located at the front, and so is the bloom.

In general, in addition to the reduced turbulence, the bloom at the front is induced by the biological responses to MZCW veering offshore during the relaxation of the northeast monsoon.

6 Conclusions

A coupled physical–biological model was developed to simulate the winter offshore bloom in the TWS during the weakening of the northeast monsoon. The model results show the geostrophic adjustment pushes the eutrophic MZCW off the coast to the middle of the TWS during the relaxation of the wind. The veering offshore of the MZCW helps to stratify the upper layer, which plays a dominant role in reducing turbulence.

From the biological aspect, the chlorophyll concentration increases in the upper layer of the western strait and the bloom appears offshore, which resembles the observations. The model diagnostic analysis reveals the bloom is induced by the reduced turbulence. The weakened turbulence reduces the vertical mixing, which mixes the phytoplankton downward. As a result, the phytoplankton accumulate in the upper layer

BGD
10, 14685–14714, 2013

where more light is available for efficient photosynthesis, which leads to the bloom. The analysis result for the bloom is further verified by the critical turbulence theory. In addition, due to the temporal lag between phytoplankton and zooplankton, the locations of maximal chlorophyll and zooplankton are inconsistent and the bloom occurs at the front.

Therefore, the mechanism of the offshore bloom in winter in the TWS is proposed and confirmed in this study. The weakening of the northeast wind causes the fresh MZCW to veer offshore, and the stratified water inhibits the turbulence in the upper layer. The reduced turbulence leads to phytoplankton accumulation within the upper layer and causes chlorophyll to increase. Finally, the biological processes are responsible for the offshore maximal chlorophyll (i.e., the bloom at the front).

Acknowledgements. This work was supported by grant (2013CB955704) from the National Major Scientific Research Program of China, grant (2013BAB04B00) from the National Key Technology R&D Program. This work was completed while Yuwu Jiang was visiting the University of Delaware during his sabbatical.

References

Chang, Y., Shimada, T., Lee, M. A., Lu, H. J., Sakaida, F., and Kawamura, H.: Wintertime sea surface temperature fronts in the Taiwan Strait, Geophys. Res. Lett., 33, L23603, doi:10.1029/2006gl027415, 2006.

da Silva, A. M., Young, C. C., and Levitus, S.: Algorithms And Procedures, in: Atlas of surface marine data 1994, NOAA atlas NESDIS 6, US Department of Commerce, USA, 74, 1994.

Fennel, K., Wilkin, J., Levin, J., Moisan, J., O'Reilly, J., and Haidvogel, D.: NItrogen cycling in the Middle Atlantic Bight: Result from a three-dimensional model, Global Biogeochem. Cy., 20, GB3007, doi:10.1029/2005GB002456, 2006.

Hu, J. Y., Kawamura, H., Li, C. Y., Hong, H. S., and Jiang, Y. W.: Review on Current and Seawater Volume Transport through the Taiwan Strait, J. Oceanogr., 66, 591–610, 2010.

BGD
10, 14685–14714, 2013

Huisman, J., Oostveen, P., and Weissing, F. J.: Critical Depth and Critical Turbulence: Two Different Mechanisms for the Development of Phytoplankton Blooms, Limnol. Oceanogr., 44, 1781–1787, 1999.
Jan, S., Chern, C. S., and Wang, J.: A numerical study of currents in the tws during winter, TAO, 9, 615–632, 1998.
Jan, S., Wang, J., Chern, C. S., and Chao, S. Y.: Seasonal variation of the circulation in the Taiwan Strait, J. Mar. Syst., 35, 249–268, 2002.
Lewis, M. R., Horne, E. P. W., Cullen, J. J., Oakey, N. S., and Platt, T.: Turbulent motions may control phytoplankton photosynthesis in the upper ocean, Nature, 311, 49–50, 1984.
Li, C., Hu, J., Jan, S., Wei, Z., Fang, G., and Zheng, Q.: Winter-spring fronts in Taiwan Strait, J. Geophys. Res., 111, C11S13, doi:10.1029/2005jc003203, 2006.
Liao, E. H., Jiang, Y. W., Li, L., Hong, H., and Yan, X. H.: The cause of the 2008 cold disaster in the Taiwan Strait, Ocean Model., 62, 1–10, 2013.
Lin, S. F., Tang, T. Y., Jan, S., and Chen, C. J.: Taiwan strait current in winter, Cont. Shelf Res., 25, 1023–1042, doi:10.1016/j.csr.2004.12.008, 2005.
Lin, X., Yan, X.-H., Jiang, Y., and Zhang, Z.: Skill Assessment of an Operational Ocean Model in the Taiwan Strait, Ocean Model., in review, 2013.
Mellor, G. L.: One-dimensional, ocean surface modeling, a problem and a solution, J. Phys. Oceanogr., 31, 790–809, 2001.
Mellor, G. L. and Yamada, T.: Development of a turbulence closure model for geophysical fluid problems, Rev. Geophys. Space Phys., 20, 851–875, 1982.
Miles, T. N. and He, R.: Temporal and spatial variability of Chl-a and SST on the South Atlantic Bight: Revisting with cloud-free reconstructions of MODIS satellite imagery, Cont. Shelf Res., 30, 1951–1962, 2010.
Morel, A. and Berthon, J. F.: Surface pigments, algal biomass profiles, and potential production of the euphotic layer: Relationships reinvestigated in view of remote-sensing applications, Limnol. Oceanogr., 34, 1545–1562, 1989.
Naik, H. and Chen, C. C. A.: Biogeochemical cycling in the Taiwan Strait, Estuar. Coast. Shelf S., 78, 603–612, doi:10.1016/j.ecss.2008.02.004, 2008.
Shchepetkin, A. F. and McWilliams, J. C.: The regional oceanic modeling system (ROMS):a split-explicit, free-surface, topography-following-coordinate oceanic model, Ocean Model., 9, 347–404, doi:10.1016/j.ocemod.2004.08.002, 2005.

BGD
10, 14685–14714, 2013

Sverdrup, H. U.: On conditions for the vernal blooming of phytoplankton, J. Conseil Int. Explot. Mer, 18, 287–295, 1953.
Taylor, J. R. and Ferrari, R.: shutdown of turbulent convection as a new criterion for the onset of spring phytoplankton blooms, Limnol. Oceanogr., 56, 2293–2307, doi:10.4319/lo.2011.56.6.2293, 2011.
Wang, J. and Chern, C. S.: On the Kuroshio branch in the Taiwan Strait during wintertime, Prog. Oceanogr., 21, 469–491, 1988.
Wang, J. and Chern, C. S.: On cold water intrusions in the eastern Taiwan Strait during the cold season, Acta Oceanogr. Taiwan., 22, 43–67, 1989.
Wang, J., Hong, H., Jiang, Y., Chai, F., and Yan, X.-H.: Summer nitrogenous nutrient transport and its fate in the Taiwan Strait: a coupled physical-biological modeling approach, J. Geophys. Res., in press, doi:10.1002/jgrc.20300, 2013.
Xing, L. Y.: Distributions of Dissolved Organic Nitrogen and Phosphorus, as well as Degree of Nutrient Consumption in the Taiwan Strait, Master, Institute of Marine Geology and Chemistry, National Sun Yat-sen University, Taiwan, 2004.
Yang, J. Y.: An oceanic current against the wind: how does Taiwan Island steer warm water into the East China Sea, J. Phys. Oceanogr., 37, 2563–2569, 2007.
Zhang, C. Y., Shang, S. L., Chen, D. W., and Shang, S. P.: Short-term Variability of the Distribution of Zhe-Min Coastal Water and Wind Forcing during Win ter Monsoon in the Taiwan Strait, J. Remote Sens., 7, 452–458, 2005.
Zhang, F. and Huang, B. Q.: Affect of hydrological characteristics for the distribution and variablity of chlorophyll A in the northern part of Taiwan Strait in winter, Mar. Sci., 24, 1–3, 2000 (in Chinese).

BGD
10, 14685–14714, 2013

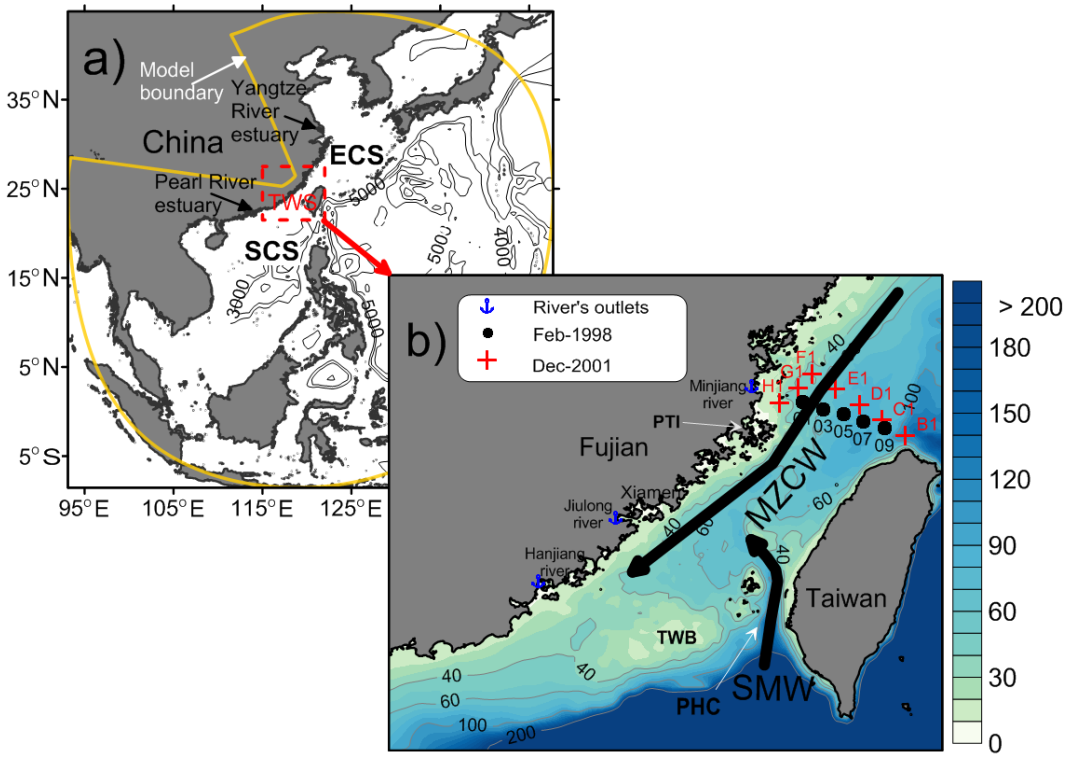

Fig. 1. (a) Model domain with isobaths (units: m). **(b)** Bathymetry (with isobaths shown) of the Taiwan Strait, which is marked by the red dashed box in **(a)**. The dots and crosses indicate the observation stations in 1998 and 2001. The blue anchor symbols indicate rivers' outlets. The thick lines indicate the main circulation in the strait in winter: MZCW for the Min-Zhe coastal water; SMW for south mixing water; PTI for Pingtan Island; PHC for the Penghu Channel; and TWB for the Taiwan Bank.

BGD
10, 14685–14714, 2013

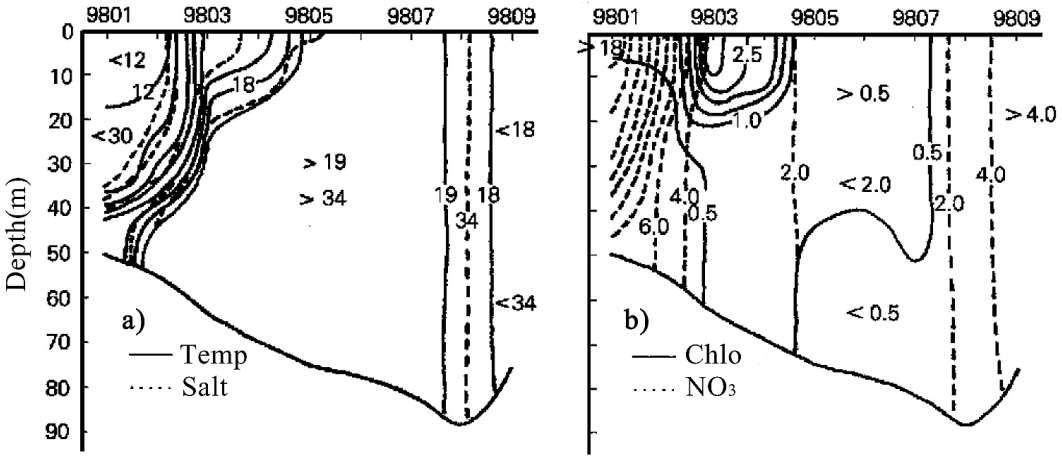

Fig. 2. Distributions of temperature (Temp; units: ˚C), salinity (Salt; units: psu), chlorophyll *a* (Chlo; units: mg m^{-3}), and NO_3 (units: mmol m^{-3}) along the observation section in February 1998. Redrawn after Zhang and Huang (2000).

BGD
10, 14685–14714, 2013

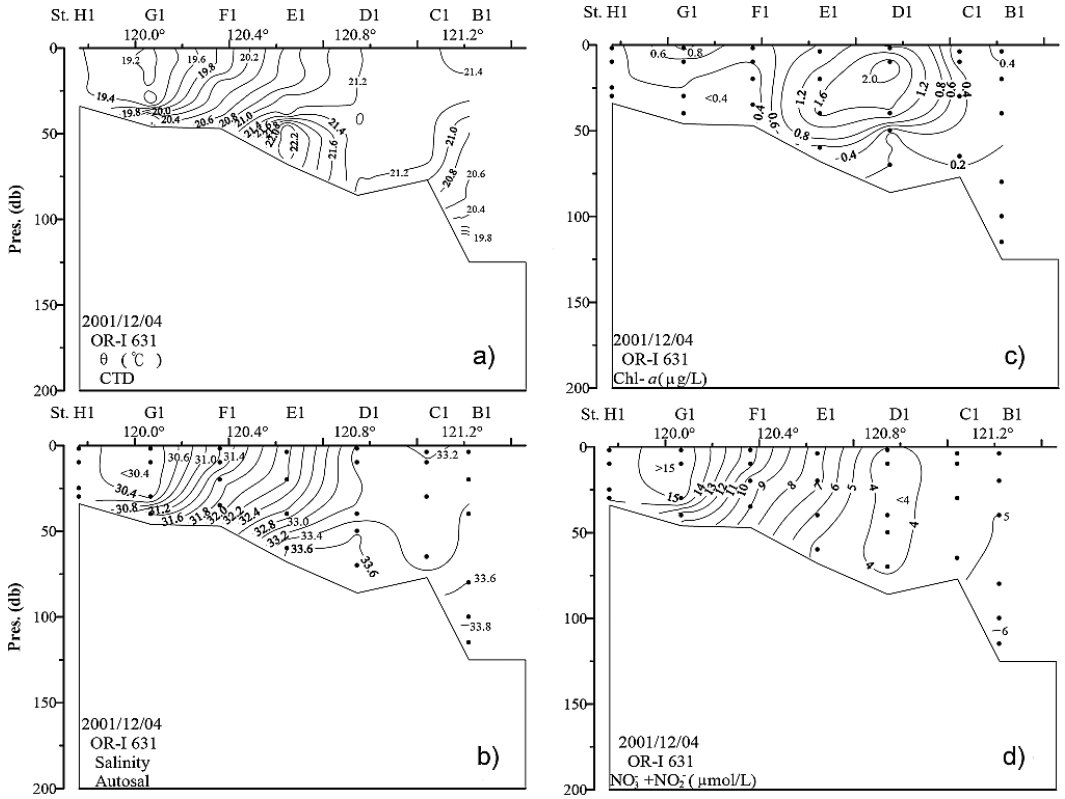

Fig. 3. Distributions of temperature **(a)**, salinity **(b)**, chlorophyll *a* **(c)**, and $NO_3 + NO_2$ **(d)** along the observation section in December 2001. Redrawn after Xing (2004) and Naik and Chen (2008).

BGD
10, 14685–14714, 2013

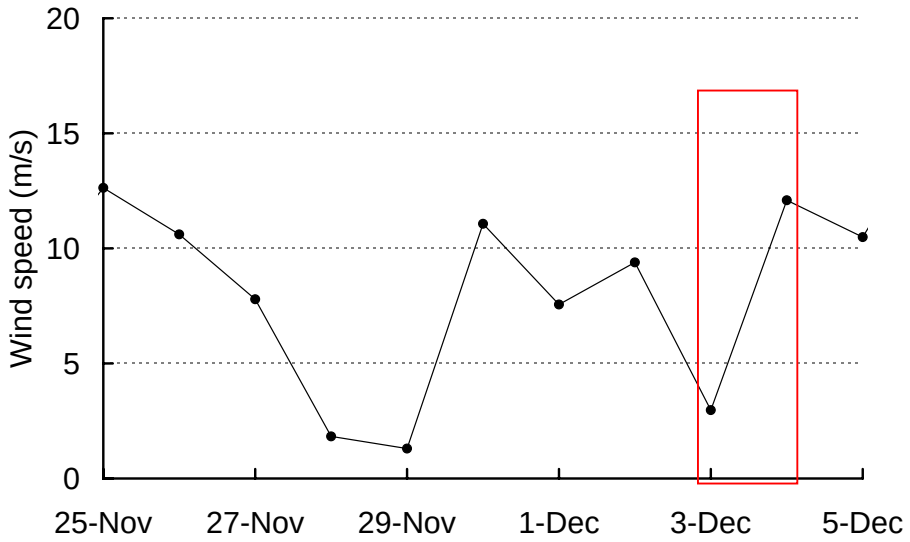

Fig. 4. Area-mean wind speed in the TWS during 25 November–5 December 2001, based on the daily-mean wind data of QuikSCAT. The red box indicates the survey period.

BGD
10, 14685–14714, 2013

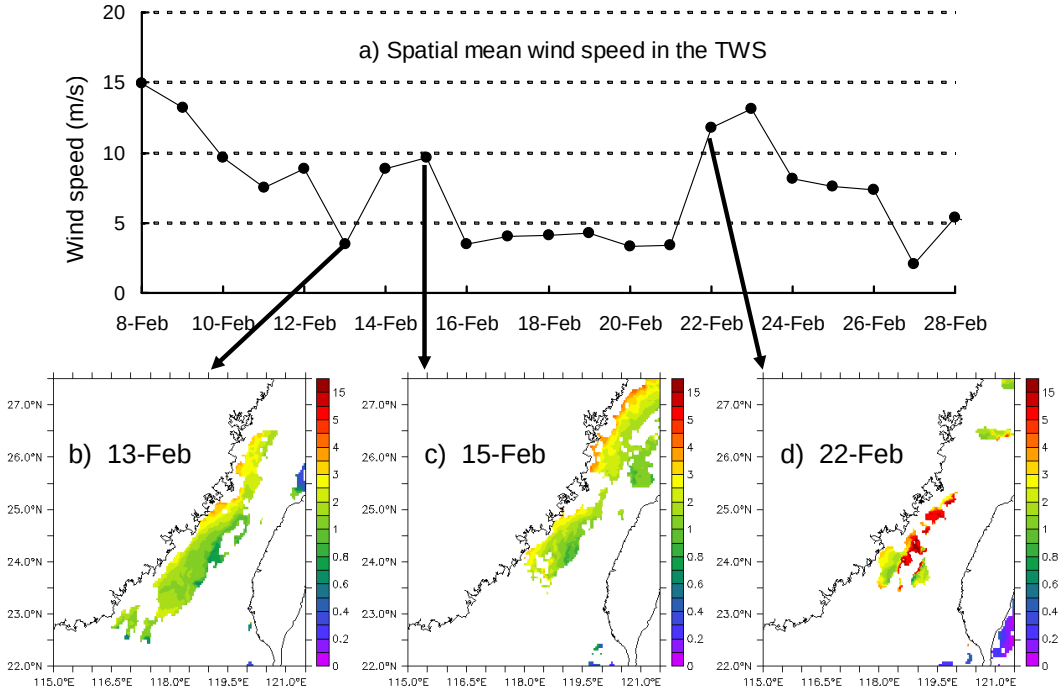

Fig. 5. Satellite observation of bloom in the TWS in February 2004. **(a)** Area-mean wind speed in the TWS, based on the daily mean wind data of QuikSCAT. **(b–d)** MODIS daily-mean sea surface chlorophyll *a* (units: mg m^{-3}).

BGD
10, 14685–14714, 2013

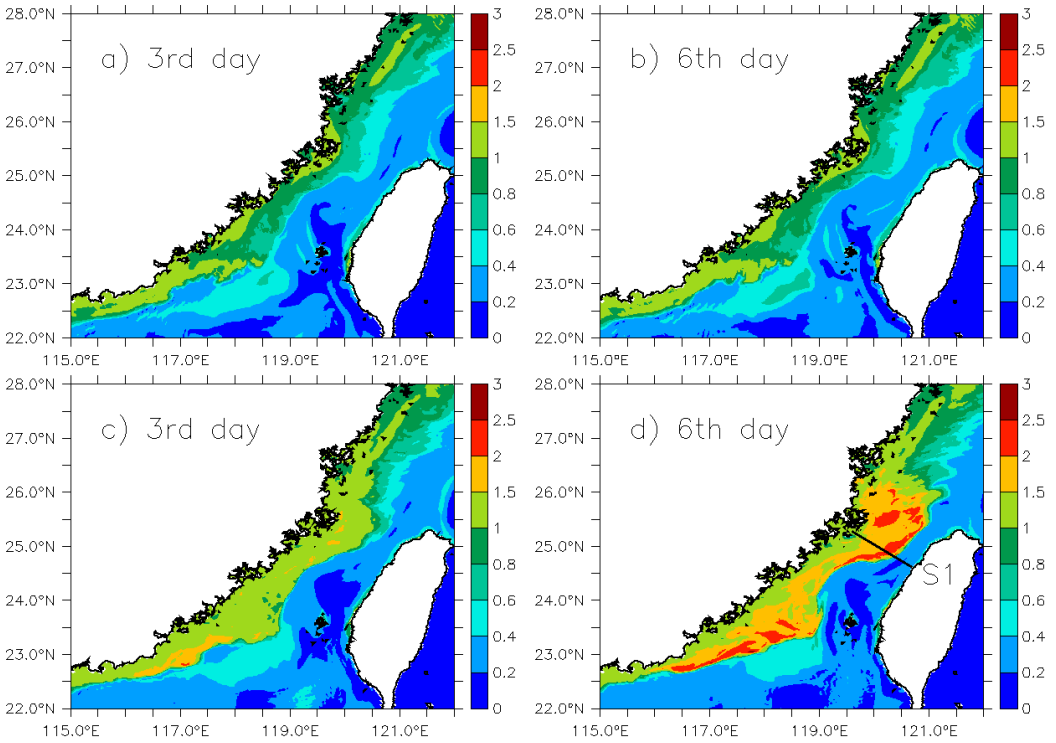

Fig. 6. Simulated surface chlorophyll *a* distributions (units: mg m^{-3}) in the climatological case **(a, b)** and relaxed-wind case **(c, d)**. The 3rd and 6th day mean 3- and 6-day spinup from January 15, respectively. The thick line in **(d)** is the sampled section S1 for Figs. 7–14.

BGD
10, 14685–14714, 2013

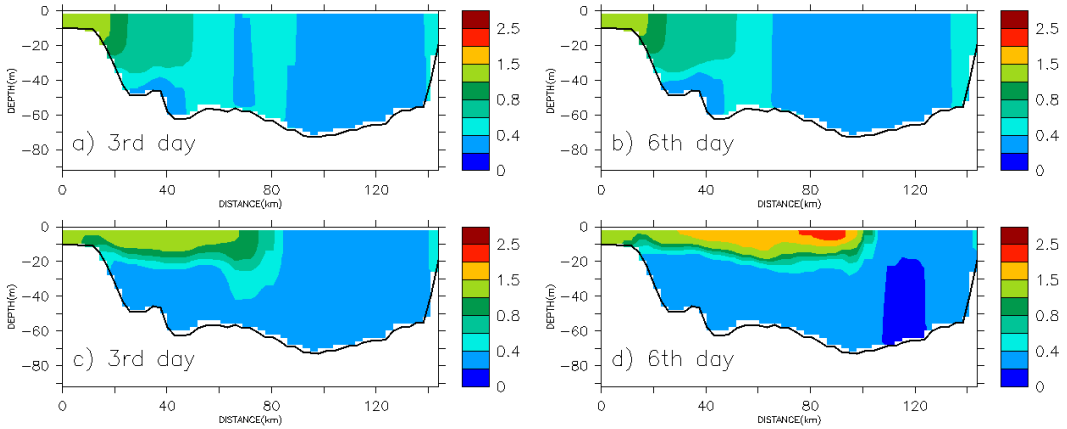

Fig. 7. Simulated chlorophyll *a* distributions (units: mg m^{-3}) along section S1 in the climatological case **(a, b)** and relaxed-wind case **(c, d)**.

BGD
10, 14685–14714, 2013

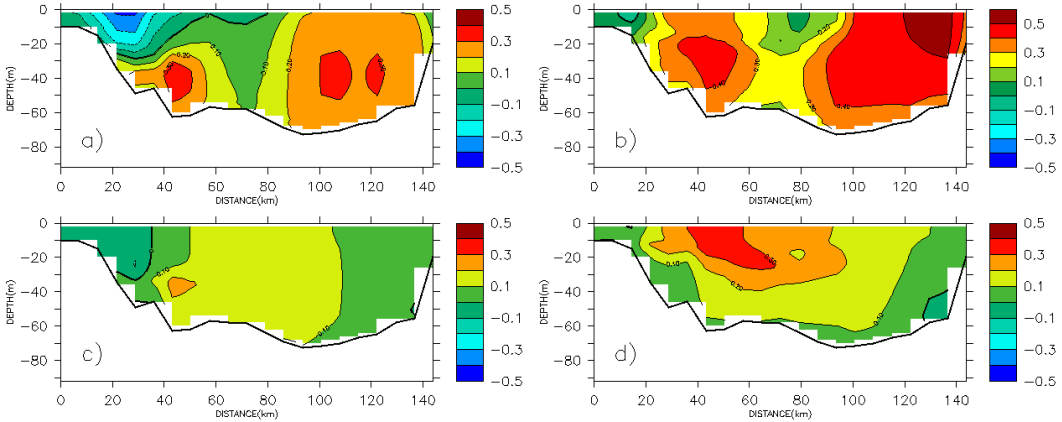

Fig. 8. Along-strait **(a, b)** and across-strait **(c, d)** velocities (units: $m\,s^{-1}$) on the 6th day along section S1 (left panel: climatological case; right panel: relaxed-wind case). The positive indicates toward the northeast direction in **(a)** and **(b)**, and the direction off the west shore in **(c)** and **(d)**.

BGD
10, 14685–14714, 2013

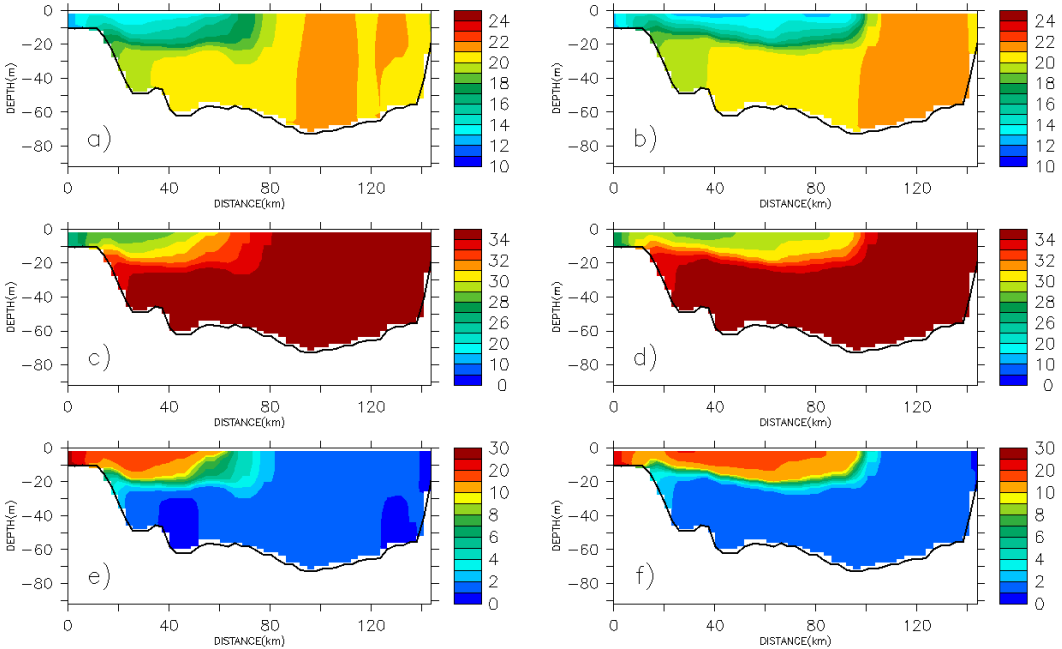

Fig. 9. Simulated distributions of temperature (**a**, **b**; units: ˚C), salinity **(c, d)** and NO_3 (**e**, **f**; units: mmol m^{-3}) along section S1 in the relaxed-wind case (left panel: on 3rd day; right panel: on 6th day).

BGD
10, 14685–14714, 2013

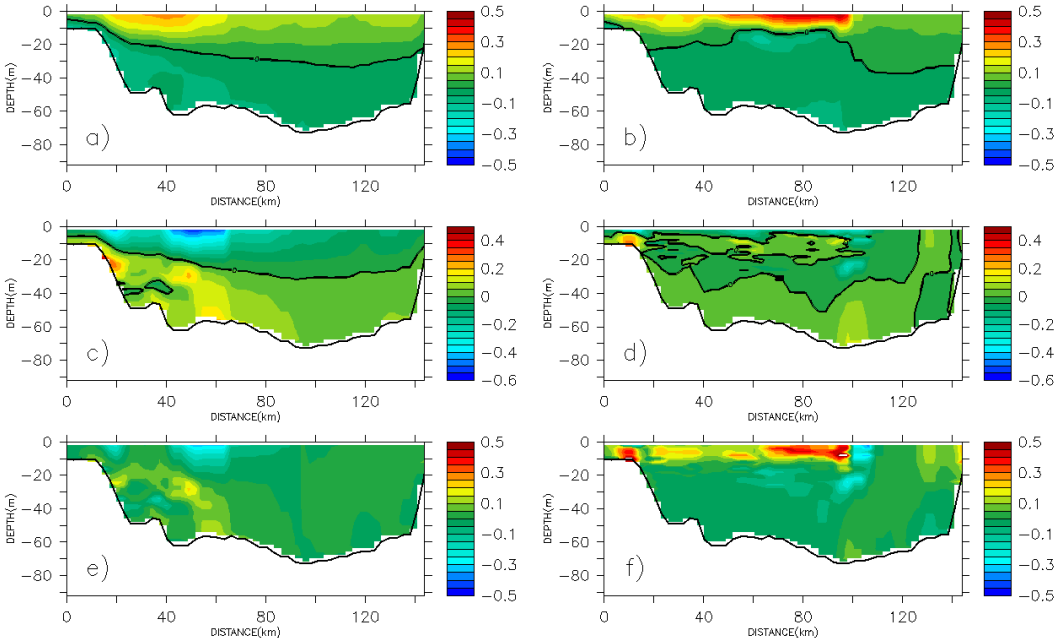

Fig. 10. Distributions (units: mg m^{-3} day^{-1}) of the net biological rate **(a, b)**, diffusion rate **(c, d)**, and net rate **(e, f)** in Eq. (1) along section S1 on the 6th day (the thick line is the zero contour). Left panel: climatological case; and right panel: relaxed-wind case.

BGD
10, 14685–14714, 2013

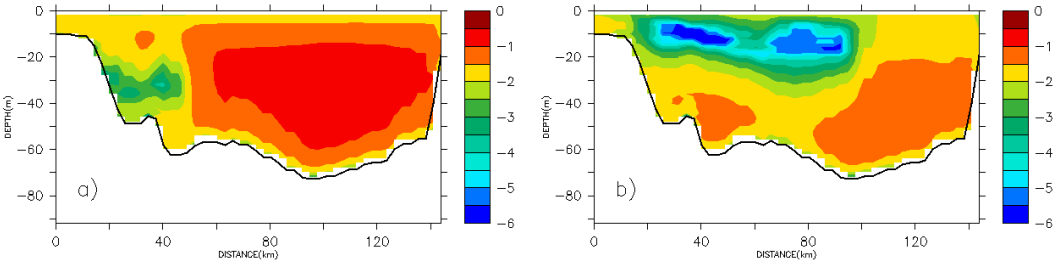

Fig. 11. Logarithm of vertical diffusion coefficient (units: $m^2\,s^{-1}$) along section S1 in the climatological case **(a)** and relaxed-wind case **(b)** on the 6th day.

BGD
10, 14685–14714, 2013

Initiation of the offshore phytoplankton bloom during winter

J. Wang et al.

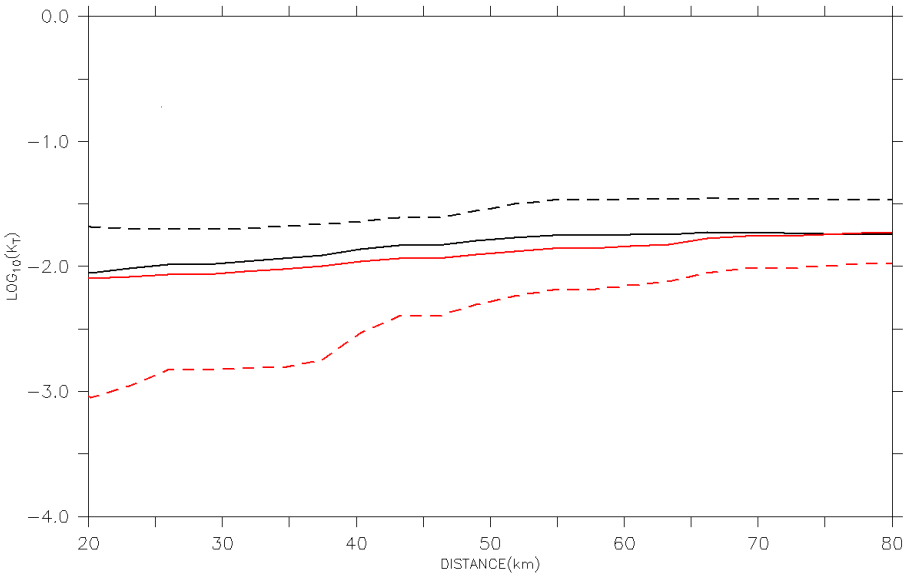

Fig. 12. Logarithm of critical turbulence and turbulence diffusion coefficient along the western part of section S1. Solid lines are the critical turbulence, and dashed lines are the diffusion coefficient in the model. The black lines present the climatological case, and the red lines present relaxed-wind case.

BGD
10, 14685–14714, 2013

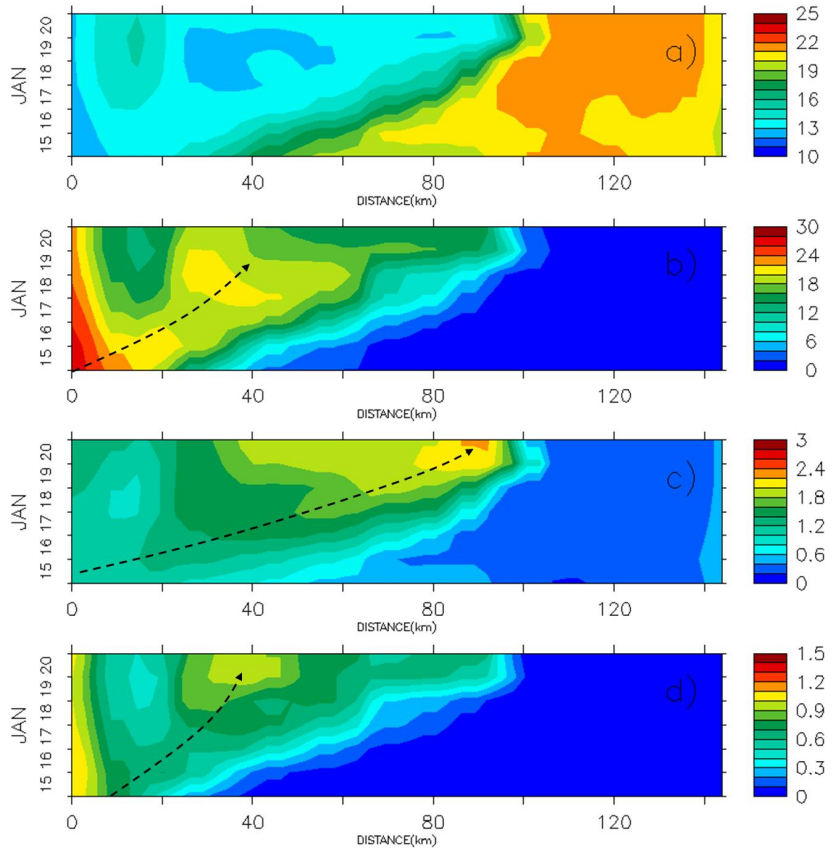

Fig. 13. Evolution of the temperature (**a**; units: °C), NO_3 (**b**; units: mmol m^{-3}), chlorophyll *a* (**c**; units: mg m^{-3}), and zooplankton (**d**; units: mmol m^{-3}) at surface along section S1 in the relaxed-wind case. The dotted vector indicates the moving trajectory of the maximum value approximately.

BGD
10, 14685–14714, 2013

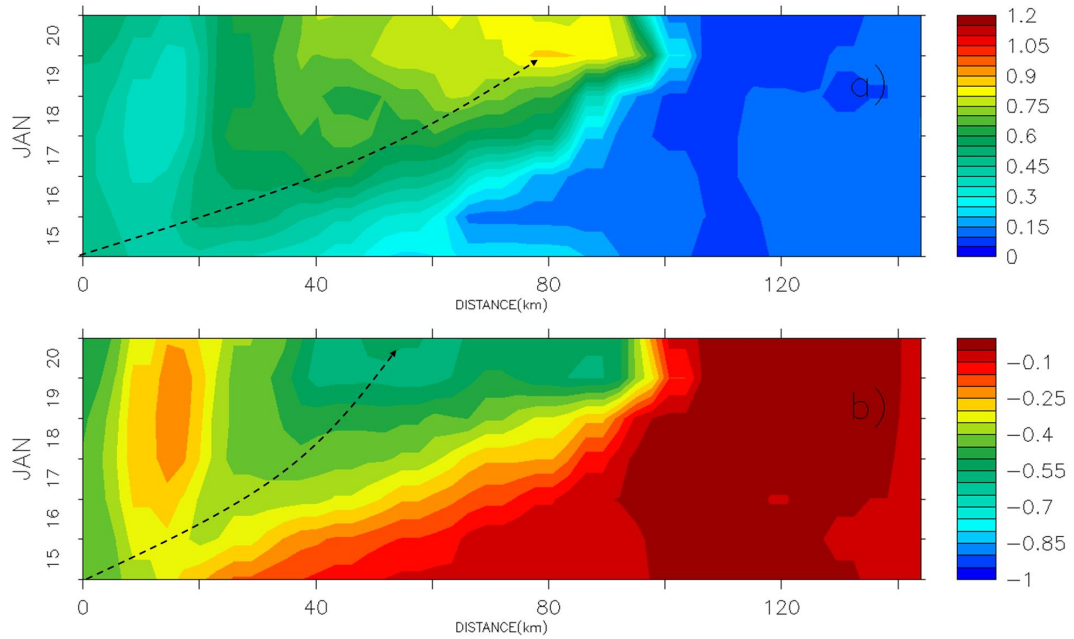

Fig. 14. Time series of phytoplankton growth **(a)** and depletion **(b)** rates (units: mg m^{-3} day^{-1}) in Eq. (1) at surface along section S1 in the relaxed-wind case. The dotted vectors approximately indicate the moving trajectory of the maximum and minimum value in **(a)** and **(b)**, respectively.

BGD
10, 14685–14714, 2013